International Journal of Rock Mechanics & Mining Sciences 128 (2020) 104281

Contents lists available at ScienceDirect

International Journal of Rock Mechanics and Mining Sciences

journal homepage: http://www.elsevier.com/locate/ijrmms

Differential poroelasticity model for wave dissipation in self-similar rocks

Lin Zhang [a,b], Jing Ba [a,c,d,**], José M. Carcione [a,e], Li-yun Fu [d]

[a] School of Earth Sciences and Engineering, Hohai University, Nanjing 211100, China
[b] College of Science, Purdue University, West Lafayette, IN 47907, USA
[c] Department of Earth and Atmospheric Sciences, University of Houston, Houston, TX 77204 USA
[d] School of Geosciences, China University of Petroleum (East China), Qingdao 266580, China
[e] Istituto Nazionale di Oceanografia e di Geofisica Sperimentale (OGS), Trieste 34010, Italy

ABSTRACT

The double-porosity theory of wave propagation in rocks considers a single scale based on soft and stiff pores, and wave attenuation occurs by local fluid flow between these pores. However, rocks exhibit more complicated fabric structures, with heterogeneities presented at multiple scales, having a self-similar fractal nature as reported. We develop a poroelasticity model to describe wave anelasticity in a fluid-saturated medium consisting of infinite components, i.e., an infinituple-porosity medium. Numerical modeling is achieved with infinite iterations, where at each iteration one component is added (a porous inclusion embedded in a porous host), analogous to the differential effective medium (DEM) theory of solid composites. By considering the self-similar structure, the properties of each component (inclusions) are scale-dependent. The example shows that the P-wave velocity dependence on frequency depends on thfractal dimension. Application of the model to sandy sea-bottom sediments shows a good agreement, with fractal dimension of 2.88.

1. Introduction

Many poroelasticity theories describe wave propagation in rocks, where the pores have different shapes and compressibilities, e.g., squirt-flow theories.[1–5] In double-porosity media,[6–11] a background medium and softer or stiffer porous inclusions are assumed, on the basis of a single heterogeneity scale. Due to the different compressibilities of host and inclusions, a P-wave induces a fluid pressure gradient and a local fluid flow (LFF).[12–14] At low frequencies, the medium is relaxed since the fluid pressure has time to equilibrate at each cycle, whereas at high frequencies the dissimilar pressures (unrelaxation) and the consequent LFF causes a medium stiffening, with the P-wave velocity increasing with frequency. This implies the dispersion and dissipation due to P-wave energy conversion to Biot slow modes.[15–17]

The poroelasticity theory has been generalized to the case of triple-porosity by Sun et al.[18] and Zhang et al.,[19] where an inclusion of a triple-layer spherical patch (with outer shells and an inner core) is considered. Each of the three components has different mineral or fluid properties. Ba et al.[20] presented a double double-porosity theory to analyze the overlapping effect of two types of heterogeneities, fabric and patchy-saturation. Although this theory considers four types of pores, it is not enough to characterize the complex structures of rocks, which generally undergo a multi-stage effect of tectonization, deposition and dissolution in geologic time, resulting in fractal pore and crack phases. Previous studies assumed uniform-to quadruple-porosity media,[7,18,20,21] where a limited kind of pore phases were assumed as inclusions embedded within a host medium.

It is believed that a reasonable model has to be fractal, i.e., statistically self-similar.[22–24] Studies were performed on the relationships between fractal geometry and thermal conductivity,[25] elastic properties,[26] permeability,[27] and electrical conductivity.[28] Pride and Masson[29] suggested a relation between wave attenuation and fractal geometry based on numerical examples, but it remains not clear if a fractal geometry can be theoretically implemented to describe wave anelasticity.

The elastic moduli of solid composites can be estimated with the differential effective medium (DEM) theory,[30–33] which usually incorporates only two components. It has been extended to multiple constituents by Han.[34] Although the DEM was applied to fluid-saturated media by Berryman,[35] wave-induced flow has not been incorporated, and consequently, wave dissipation has been neglected.

In analogy with the DEM theory for a solid, we present an extended approach for fluid-saturated media, where we add one component in each iteration. The complex moduli of an infinituple-porosity medium are then obtained after infinite iterations, and the differential equations of wave propagation are derived. To study the physics, we perform a plane-wave analysis, giving the wave anelastic properties of the medium as a function of the fractal dimension. Finally, the theory is applied to broad-band measurements in sea-bottom sediments.

* Corresponding author. School of Earth Sciences and Engineering, Hohai University, Nanjing, 211100, China.
E-mail addresses: jingba@188.com, jba@hhu.edu.cn (J. Ba).

https://doi.org/10.1016/j.ijrmms.2020.104281
Received 22 December 2019; Received in revised form 22 February 2020; Accepted 25 February 2020
Available online 4 March 2020
1365-1609/

2. Theory

2.1. Differential poroelasticity model

The Biot-Rayleigh theory[8] for wave propagation in double-porosity rocks assumes one component (inclusion) embedded in a host medium. The governing equations for wave propagation are based on the Hamilton principle.

In analogy with the DEM theory, where inclusion and host are solids, we consider spherical porous inclusions and host (fluid-saturated). The procedure is illustrated in Fig. 1. One component is considered as the initial host, and the composite is built by a number of incremental additions of inclusions. In each step, the phase estimated from the last addition is taken as the host, and inclusions are incrementally added by assuming a dilute concentration. The inclusions at different additions can be distinct. In this manner, an infinituple-porosity medium is obtained after infinite additions. The dry-composite moduli are determined by the differential scheme as in Berryman,[36]

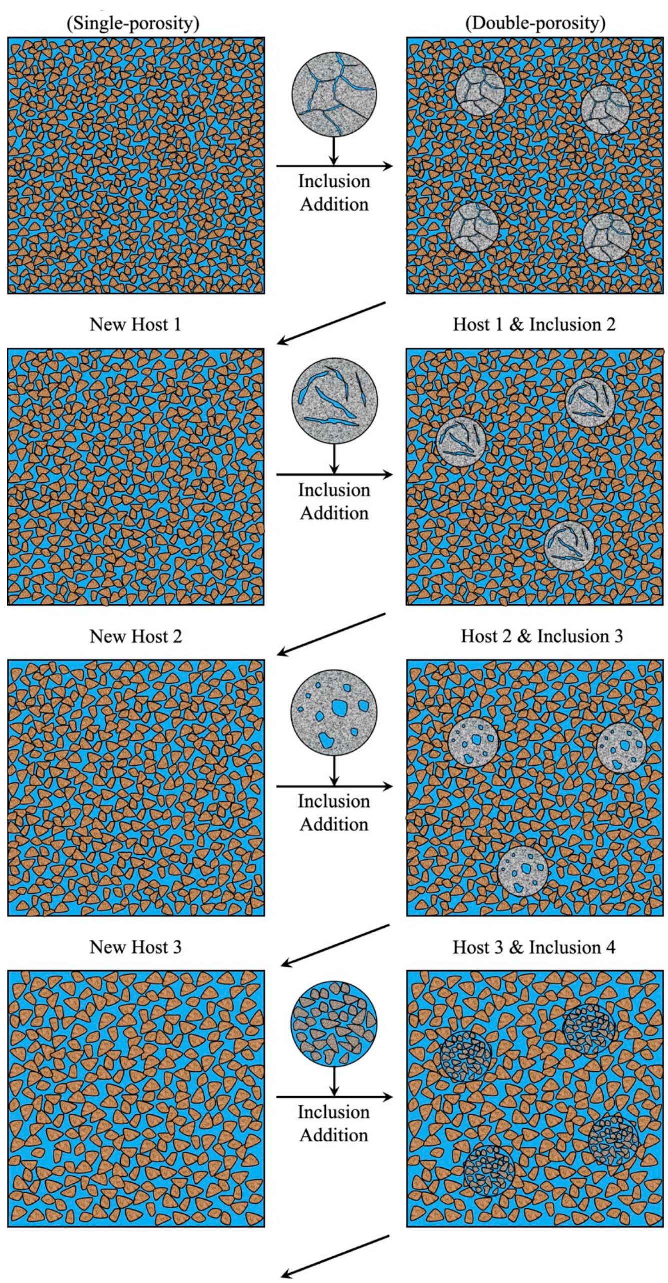

Fig. 1. The iterative construction process of the differential poroelasticity model.

$$dK_b(v_I) = \frac{(K_{bI} - K_b)L_1(v_I)}{1 - v_I} dv_I \tag{1a}$$

$$dG_b(v_I) = \frac{(G_{bI} - G_b)L_2(v_I)}{1 - v_I} dv_I \tag{1b}$$

where $K_b(v_I = 0) = K_{bH}$ and $G_b(v_I = 0) = G_{bH}$, K_{bH} and G_{bH} (K_{bI} and G_{bI}) are the dry-rock bulk and shear moduli of the initial host (inclusions), respectively, v_I is the volume fraction of inclusions, and L_1 and L_2 are the polarization factors for the bulk and shear moduli, respectively.[37]

At each addition, the double-porosity model with the host absolute porosity φ and the incremental porosity $d\varphi$, ($d\varphi = \varphi_I dv_I$, and φ_I is the matrix porosity of the inclusions) is applied to compute the complex moduli of the composite. Then, the differential equations for wave propagation are

$$\begin{aligned}
&(N + NSd\varphi)\nabla^2\mathbf{u} + (A+N)\nabla e + (A_d + NS)d\varphi\nabla e + Q_H\varphi\nabla(\xi_H + \zeta d\varphi) \\
&\quad + R_H\left(\frac{Q_I}{K_f} - \frac{Q_I}{K_s} - 1\right)d\varphi\nabla\xi_H + Q_I d\varphi\nabla(\xi_I - \varphi\zeta) \\
&\quad = \rho_{00}\ddot{\mathbf{u}} + (\rho_{00}S - \rho_s - \rho_{02})d\varphi\ddot{\mathbf{u}} + \rho_{01}\varphi\ddot{\mathbf{U}}_H + \rho_{01}\varphi Sd\varphi\ddot{\mathbf{U}}_H + \rho_{02}d\varphi\ddot{\mathbf{U}}_I \\
&\quad + \frac{\varphi\varphi_H\eta}{\kappa_H}(\dot{\mathbf{u}} - \dot{\mathbf{U}}_H) + \frac{\varphi\varphi_H\eta}{\kappa_H}Sd\varphi(\dot{\mathbf{u}} - \dot{\mathbf{U}}_H) + \frac{\varphi_I\eta d\varphi}{\kappa_I}(\dot{\mathbf{u}} - \dot{\mathbf{U}}_I)
\end{aligned} \tag{2a}$$

$$\begin{aligned}
&Q_H\nabla e + R_H\nabla(\xi_H + \zeta d\varphi) + \frac{R_H}{\varphi}\left(\frac{1}{\beta}\nabla\xi_H - \nabla e\right)d\varphi \\
&\quad = \left(1 + \frac{R_H}{\varphi}\left(\frac{1}{\beta K_f} - \frac{1}{K_s}\right)d\varphi\right)\left(\rho_{01}\ddot{\mathbf{u}} + \rho_{11}\ddot{\mathbf{U}}_H - \frac{\varphi_H\eta}{\kappa_H}(\dot{\mathbf{u}} - \dot{\mathbf{U}}_H)\right)
\end{aligned} \tag{2b}$$

$$Q_I\nabla e + R_I\nabla(\xi_I - \varphi\zeta) = \rho_{02}\ddot{\mathbf{u}} + \rho_{22}\ddot{\mathbf{U}}_I - \frac{\varphi_I\eta}{\kappa_I}(\dot{\mathbf{u}} - \dot{\mathbf{U}}_I) \tag{2c}$$

$$(Q_H e + R_H(\xi_H + \zeta d\varphi)) - (Q_I e + R_I(\xi_I - \varphi\zeta)) = \frac{1}{3}r^2\varphi\varphi_I\left(\frac{\rho_f}{\varphi_H}\ddot{\zeta} + \frac{\eta}{\kappa_H}\dot{\zeta}\right) \tag{2d}$$

where $\mathbf{u}$, $\mathbf{U}_H$ and $\mathbf{U}_I$ are the solid displacement, fluid displacement in the host medium and fluid displacement in the inclusions, respectively, and e, ξ_H and ξ_I are the corresponding displacement divergence fields. The scalar ζ represents the variation of fluid content between the host and inclusions. φ_H is the matrix porosity of the host. κ_H and κ_I are the permeabilities of the host and inclusions, respectively. r is the inclusion radius, and η is the fluid viscosity. K_s (K_f) is the grain (fluid) bulk modulus. ρ_s is the mineral (or grain) density. The derivation of equation (2) is given in Appendix A. The stiffness coefficients A, A_d, N, Q_H, Q_I, R_H, R_I, S and density coefficients ρ_{00}, ρ_{01}, ρ_{02}, ρ_{11}, ρ_{22} are given in Appendix B.

The P- and S-wave complex wave numbers (k_P and k_S) are obtained by a plane wave analysis in equation (2). Then, the complex bulk and shear moduli are

$$K_{sat} = ((1 - \varphi - d\varphi)\rho_s + (\varphi + d\varphi)\rho_f)\left(\frac{\omega}{k_P}\right)^2 - \frac{4}{3}G_{sat}, \tag{3a}$$

$$G_{sat} = ((1 - \varphi - d\varphi)\rho_s + (\varphi + d\varphi)\rho_f)\left(\frac{\omega}{k_S}\right)^2, \tag{3b}$$

where ρ_f is the fluid density and ω is the angular frequency.

The Gassmann equation[38] is applied to compute the dry-rock complex moduli at the end of each addition, used as the moduli of the new host for the next addition:

$$\frac{K_{sat}}{K_s - K_{sat}} = \frac{K_b}{K_s - K_b} + \frac{K_f}{(\varphi + d\varphi)(K_s - K_f)}, \tag{4a}$$

$$G_b = G_{sat}. \tag{4b}$$

Using equations (1)–(4) at each addition, the process consists of infinite steps, where at each step the host is assumed homogeneous and anelastic. The infinituple-porosity model is realized if the inclusion phases are distinct at each addition. At the end, the wave velocity and attenuation are computed from the last complex wave number.

2.2. Double-porosity medium

A discretization of the process actually leads to finite additions. In the particular case that all the steps assume the same type of inclusion, a double-porosity medium is obtained. Let us consider an example, where the bulk modulus of the grain is 38 GPa, the initial host bulk/shear modulus is 17GPa/15 GPa, the inclusion bulk/shear modulus is 1.7 GPa/1.5 GPa, the grain density is 2650 kg/m^3, the fluid bulk modulus is 2.5 GPa, the fluid density is 1040 kg/m^3, the fluid viscosity is 0.001 Pa•s, the initial host porosity/permeability is 0.15/0.01 D, the inclusion porosity/permeability is 0.08/1 D, the total inclusion volume ratio is 0.1, and the inclusion radius is 0.01 m. The results for $n = 1$, 25, 50, and 100 additions are shown in Fig. 2. The low-frequency limit of the P-wave velocity is given in Fig. 2a, where the dry-rock moduli are determined by the classical DEM model, and Gassmann equation for fluid substitution is used to obtain the properties of the saturated medium.

Use of one addition ($n = 1$) leads to an underestimation of the P-wave velocity (both at the low and high frequency limits) and attenuation, similar to the results of the classical DEM theory,[34] where a great deviation is observed between the results of 1-addition and multi-addition. With the increase of n, the 25-, 50-, and 100-addition results of P-wave velocity and attenuation approach to the same limits at low- and high-frequency ends. Fig. 2a shows that the P-wave velocities at low frequency agree with Gassmann equation. The convergence with increasing n and the consistency with Gassmann equation validate the theory. The dispersion and attenuation caused by the LFF occurs at a narrower band with increasing n, indicating a single-scale inclusion cannot explain the broadband dispersion and attenuation of field observations. The dispersion due to the Biot global fluid flow (GFF) is weak in the ultrasonic band in Fig. 2a, and correspondingly, the attenuation is also weak (Fig. 2b).

We also consider the intermediate results of 5, 10, 15, and 20 additions in the 25-addition case, shown as dashed curves in Fig. 2. With the increasing addition of soft inclusions, the P-wave velocity decreases at the low frequency limit. In contrast, the P-wave velocity at high frequencies significantly increases when n increases from 5 to 15, and then slightly decreases when n increases from 15 to 20. The LFF P-wave attenuation peak increases with each iteration, and correspondingly the relaxation frequency slightly shifts to the low frequencies. A continuous addition of inclusions results in a stronger stiffening effect of the rock and more dissipation.

3. Wave propagation in fractal rocks

3.1. Scale-dependent infinituple-porosity theory

If the inclusion at each iteration is different, the resulting model is scale-dependent. Therefore, $d\varphi = \varphi'(r)dr$. For an infinituple-porosity model, the governing equations of wave propagation are expressed by an integral scheme:

$$\overline{N}\nabla^2\mathbf{u} + (\overline{A}+\overline{N})\nabla e + \overline{Q}_H\varphi\nabla\left(\xi_H + \int_0^\infty \zeta\varphi'(r)dr\right) + \int_0^\infty \overline{Q}_I\varphi'(r)\nabla(\xi_I - \varphi\zeta)dr$$
$$= \overline{\rho}_{00}\ddot{\mathbf{u}} + \overline{\rho}_{01}\varphi\ddot{\mathbf{U}}_H + \int_0^\infty \overline{\rho}_{02}\varphi'(r)\ddot{\mathbf{U}}_I dr + \frac{\varphi\overline{\varphi}_H\eta}{\overline{\kappa}_H}(\dot{\mathbf{u}} - \dot{\mathbf{U}}_H) + \eta\int_0^\infty \frac{\varphi_I}{\kappa_I}(\dot{\mathbf{u}} - \dot{\mathbf{U}}_I)\varphi'(r)dr, \tag{5a}$$

$$\overline{Q}_H\nabla e + \overline{R}_H\nabla\left(\xi_H + \int_0^\infty \varphi'(r)\zeta dr\right) = \overline{\rho}_{01}\ddot{\mathbf{u}} + \overline{\rho}_{11}\ddot{\mathbf{U}}_H - \frac{\overline{\varphi}_H\eta}{\overline{\kappa}_H}(\dot{\mathbf{u}} - \dot{\mathbf{U}}_H), \tag{5b}$$

$$\overline{Q}_I\nabla e + \overline{R}_I\nabla(\xi_I - \varphi\zeta) = \overline{\rho}_{02}\ddot{\mathbf{u}} + \overline{\rho}_{22}\ddot{\mathbf{U}}_I - \frac{\varphi_I\eta}{\kappa_I}(\dot{\mathbf{u}} - \dot{\mathbf{U}}_I), \tag{5c}$$

$$\left(\overline{Q}_H e + \overline{R}_H\left(\xi_H + \int_0^\infty \zeta\varphi'(r)dr\right)\right) - (\overline{Q}_I e + \overline{R}_I(\xi_I - \varphi\zeta)) = \frac{1}{3}r^2\varphi\varphi_I\left(\frac{\rho_f}{\overline{\varphi}_H}\ddot{\zeta} + \frac{\eta}{\overline{\kappa}_H}\dot{\zeta}\right), \tag{5d}$$

where φ_I and κ_I are relevant with the inclusions at the scale r. $\overline{\varphi}_H$, $\overline{\kappa}_H$, the stiffnesses $\overline{A}$, $\overline{N}$, $\overline{Q}_H$, $\overline{Q}_I$, $\overline{R}_H$, $\overline{R}_I$ and the density coefficients $\overline{\rho}_{00}$, $\overline{\rho}_{01}$ $\overline{\rho}_{02}$, $\overline{\rho}_{11}$, $\overline{\rho}_{22}$ can be determined as in the discretization procedure illustrated in Section 2.1.

3.2. Example of self-similar porous rocks

Natural or synthetic rocks can be assumed fractal and statistically self-similar.[22–24,39] By considering a self-similar medium, the volume fraction of inclusions is dependent on its scale, based on the porosity-scale relation presented by Rieu and Perrier[40]:

$$v_I = 1 - \left(\frac{r_{\min}}{r_{\max}}\right)^{D_E - D_f} \tag{6}$$

where D_E is the Euclidean dimension, and D_f is the fractal dimension satisfying $2<D_f<3$, which represents the degree of filling of pore spaces or fabric grains in a self-similar rock. $r_{\min}$ and $r_{\max}$ are the minimum and maximum inclusion radii of the self-similarity range, respectively. The P-wave velocity and attenuation as functions of frequency are shown in Fig. 3. The rock is assumed fractal in the scale ranges of [0.00001, 0.05] and [0.000001, 0.05] m. The total inclusion volume ratio is equal to 0.1, and the volume fraction of each addition is determined from Equation (6). The other rock properties are the same as in Fig. 2.

A comparison between the curves with different fractal parameters and the same scale range shows that when D_f increases, the P-wave velocity decreases, and the frequency range of the dispersion/attenuation is broader. A larger D_f indicates that the inclusions are more uniformly distributed (finely textured). For a self-similar rock, the dispersion and attenuation due to LFF are significant in the full frequency range, and their dependence depends on the fractal dimension D_f. Fig. 3a also shows that at the same D_f, the P-wave velocity decreases with a larger scale range of the radius.

3.3. Example. Marine sediments

The fractal model is applied to broadband data recorded on sandy sea-bottoms (summarized by[41]). These sediments are from 20 different sites around the world and the measurements span the frequency range of 50 Hz–400 kHz. The corresponding porosity and permeability are in the range of 0.36–0.47 and 0.65 × 10^{-11}-10 × 10^{-11} m^2, respectively. Moreover, the media are composed primarily of fine sand or sand-silt mixture (low frequency experiment)[42,43] and coarse-to-medium sand (high frequency experiment).[44,45] The grain bulk modulus K_s is 32 GPa,

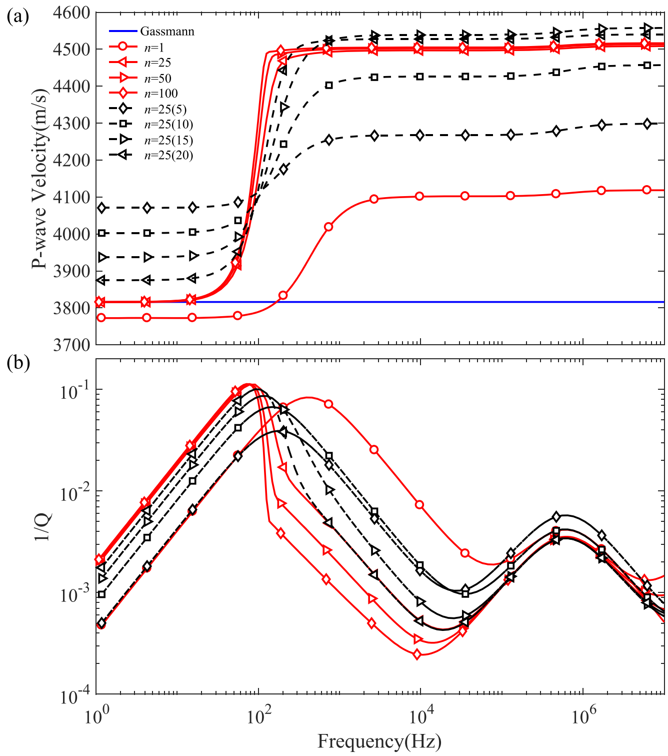

Fig. 2. P-wave velocity and attenuation as a function of frequency corresponding to n = 1, 25, 50 and 100. Results for 5, 10, 15, and 20 iterations (additions) in the 25-addition case are also given.

due to the presence of silt, and the grain density ρ_s is 2650 kg/m^3.

The rock properties are consistent with theoretical considerations and/or experiments.[46,47] Let us assume that the host is a sand with a dry-rock bulk modulus of 0.5 GPa, a dry-rock shear modulus of 0.03 GPa, a porosity of 0.395 and a permeability of 0.8 $\times$ 10^{-11} m^2.

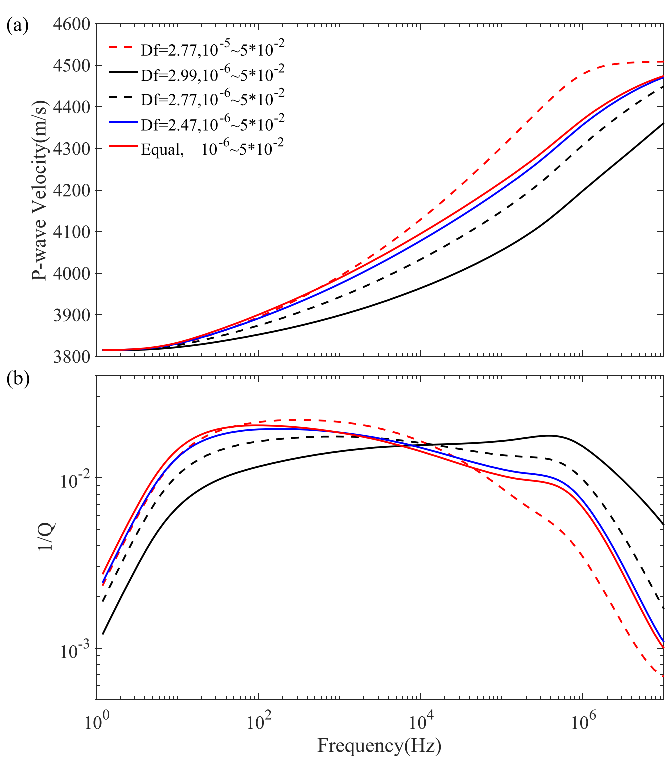

Fig. 3. Simulated P-wave velocity and attenuation as a function of frequency with respect to D_f and scale ranges [0.00001, 0.05] and [0.000001, 0.05] m.

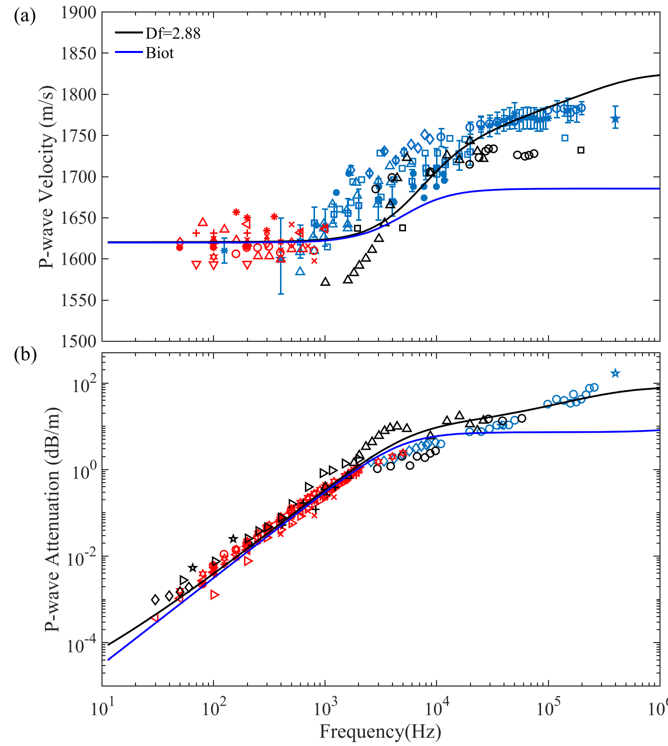

Fig. 4. P-wave velocity and attenuation predictions by the Biot model (blue curve) and differential poroelasticity model (black curve) in comparison to the full frequency range measurements of sandy sea-bottoms. Different symbols represent the datasets by different authors in literature (Data details are given in the Data in brief). (For interpretation of the references to colour in this figure legend, the reader is referred to the Web version of this article.)

Grain/particle aggregates with different degrees of compaction are considered as inclusions, with a dry-rock bulk modulus of 0.22 GPa, a dry-rock shear modulus of 0.028 GPa, a porosity of 0.5 and a permeability of 1 $\times$ 10^{-11} m^2. Moreover, the fluid (brine) bulk modulus, density and viscosity are 2.14 GPa, 1040 kg/m^3 and 0.001 Pa s, respectively.[48] It is assumed that the average porosity is 0.4 and it is fractal in the scale range of [0.003, 30] m. We use the fractal dimension D_f as a fitting parameter and the results are obtained by a least-square regression method.

The data compared to the predictions of the fractal and classical Biot models are shown in Fig. 4. Both models agree with the observed P-wave velocities and attenuation at low frequencies (<1 kHz), but the Biot model fails to match the measurements at frequencies higher than 1 kHz, where the GFF peak of Biot is not the dominant mechanism for anelasticity in this kind of loose media (sand/clay). It is clear that the significant contribution is given by the LFF at multiple scales. Due to this discrepancy with the Biot model, Chotiros and Isakson[48] and Kimura[4] incorporated a squirt-flow mechanism. However, this model cannot be applied to simulate wave anelasticity in the full frequency range. On the other hand, the fractal model provides a reasonable description for D_f = 2.88. The fractal dimension agrees with previous reported values in the range 2.49–2.89 for rocks.[22,23]

4. Conclusions

The differential poroelasticity model is presented to describe wave propagation and dissipation in fluid-saturated rocks, which consists of infinite components. The method to obtain the differential equations of motion follows the classical DEM theory for composites made of solid phases, to obtain the dry-rock moduli iteratively. Then, the double-porosity theory is used to incorporate the wave-induced fluid-flow loss mechanism at each iteration. Since the inclusions in different additions can be distinct, an infinituple-porosity model is realized. By assuming that the inclusion properties are scale-dependent and fractal, a self-similar medium is realized. The example shows that wave anelasticity is present in a broad frequency range and depends on the fractal dimension. Then, the model is applied to broad-band measurements of acoustic waves in marine sediments. The comparisons between the theoretical predictions and the data yields a fractal dimension of 2.88, in agreement with previous results. The model of this work is derived by considering one fractal dimension. It can be generalized to a more complete model (i.e. with more fractal dimensions) in a future study, so that the natural rocks with more complex geometries can be characterized.

Declaration of competing interest

The authors declare that to their knowledge they have no personal interest or relations with academic or private Institutions that may have influenced the contents of this paper.

Acknowledgements

The authors are grateful to the support of the National Natural Science Foundation of China (41974123),the Fundamental Research Funds for the Central Universities (B200203010), Jiangsu Innovation and Entrepreneurship Plan andSpecially-Appointed Professor Plan of Jiangsu Province. The details of measurement data associated with modeling are given in the Data in brief.

Appendix A. Derivation process of Equation (2)

For a double-porosity medium, the Biot-Rayleigh theory[8] assumes one component (inclusion) embedded in a host medium. In the differential scheme, the host absolute porosity is φ, while the incremental absolute porosity for inclusion addition is $d\varphi$. The governing equations for wave propagation are

$$\begin{aligned}&\tilde{N}\nabla^2\mathbf{u}+(\tilde{A}+\tilde{N})\nabla e+\tilde{Q}_1\nabla(\xi_H+\zeta d\varphi)+\tilde{Q}_2\nabla(\xi_I-\varphi\zeta)\\&=\tilde{\rho}_{00}\ddot{\mathbf{u}}+\tilde{\rho}_{01}\ddot{\mathbf{U}}_H+\tilde{\rho}_{02}\ddot{\mathbf{U}}_I+\tilde{b}_1(\dot{\mathbf{u}}-\dot{\mathbf{U}}_H)+\tilde{b}_2(\dot{\mathbf{u}}-\dot{\mathbf{U}}_I),\end{aligned} \tag{A1a}$$

$$\tilde{Q}_1\nabla e+\tilde{R}_1\nabla(\xi_H+\zeta d\varphi)=\tilde{\rho}_{01}\ddot{\mathbf{u}}+\tilde{\rho}_{11}\ddot{\mathbf{U}}_H-\tilde{b}_1(\dot{\mathbf{u}}-\dot{\mathbf{U}}_H), \tag{A1b}$$

$$\tilde{Q}_2\nabla e+\tilde{R}_2\nabla(\xi_I-\varphi\zeta)=\tilde{\rho}_{02}\ddot{\mathbf{u}}+\tilde{\rho}_{22}\ddot{\mathbf{U}}_I-\tilde{b}_2(\dot{\mathbf{u}}-\dot{\mathbf{U}}_I), \tag{A1c}$$

$$(\tilde{Q}_1\nabla e+\tilde{R}_1\nabla(\xi_H+\zeta d\varphi))d\varphi-\varphi(\tilde{Q}_2\nabla e+\tilde{R}_2\nabla(\xi_I-\varphi\zeta))=\frac{1}{3}r^2\varphi^2\varphi_I d\varphi\left(\frac{\rho_f}{\varphi_H}\ddot{\zeta}+\frac{\eta}{\kappa_H}\dot{\zeta}\right). \tag{A1d}$$

The stiffness coefficients $\tilde{A}, \tilde{N}, \tilde{Q}_1, \tilde{Q}_2, \tilde{R}_1, \tilde{R}_2$, density coefficients $\tilde{\rho}_{00}, \tilde{\rho}_{01}, \tilde{\rho}_{02}, \tilde{\rho}_{11}, \tilde{\rho}_{22}$ and dissipation coefficients $\tilde{b}_1, \tilde{b}_2$ are dependent on φ and $d\varphi$,[8] which are expressed as

$$\begin{aligned}\tilde{A}=(1-\varphi-d\varphi)K_s-\frac{2}{3}\tilde{N}&-\frac{\beta\varphi(1-\varphi-d\varphi-K_b/K_s)K_s^2/K_f}{\beta(1-\varphi-d\varphi-K_b/K_s)+K_s/K_f(\beta\varphi+d\varphi)}\\&-\frac{(1-\varphi-d\varphi-K_b/K_s)K_s^2/K_f d\varphi}{1-\varphi-d\varphi-K_b/K_s+K_s/K_f(\beta\varphi+d\varphi)},\end{aligned} \tag{A2a}$$

$$\tilde{N}=G_b, \tag{A2b}$$

$$\tilde{Q}_1=\frac{\beta(1-\varphi-d\varphi-K_b/K_s)\varphi K_s}{\beta(1-\varphi-d\varphi-K_b/K_s)+K_s/K_f(\beta\varphi+d\varphi)}, \tag{A2c}$$

$$\tilde{Q}_2=\frac{(1-\varphi-d\varphi-K_b/K_s)\varphi K_s}{1-\varphi-d\varphi-K_b/K_s+K_s/K_f(\beta\varphi+d\varphi)}, \tag{A2d}$$

$$\tilde{R}_1=\frac{(\beta\varphi+d\varphi)\varphi K_s}{\beta(1-\varphi-d\varphi-K_b/K_s)+K_s/K_f(\beta\varphi+d\varphi)}, \tag{A2e}$$

$$\tilde{R}_2=\frac{(\beta\varphi+d\varphi)K_s d\varphi}{1-\varphi-d\varphi-K_b/K_s+K_s/K_f(\beta\varphi+d\varphi)}, \tag{A2f}$$

$$\beta=\frac{\varphi_I}{\varphi_H}\left[\frac{1-(1-\varphi_H)K_s/K_{bH}}{1-(1-\varphi_I)K_s/K_{bI}}\right], \tag{A2g}$$

$$\tilde{\rho}_{00}=(1-\varphi-d\varphi)\rho_s-\tilde{\rho}_{01}-\tilde{\rho}_{02}, \tag{A2h}$$

$$\tilde{\rho}_{01}=\varphi\rho_f-\tilde{\rho}_{11}, \tag{A2i}$$

$$\tilde{\rho}_{02}=\rho_f d\varphi-\tilde{\rho}_{22}, \tag{A2j}$$

$$\tilde{\rho}_{11}=\alpha_H\rho_f\varphi, \tag{A2k}$$

$$\tilde{\rho}_{22}=\alpha_I\rho_f d\varphi, \tag{A2l}$$

$$\tilde{b}_1 = \frac{\varphi\varphi_H\eta}{\kappa_H}, \tag{A2m}$$

$$\tilde{b}_2 = \frac{\varphi_I\eta d\varphi}{\kappa_I}. \tag{A2n}$$

where α_H and α_I are tortuosities of the host and inclusions, respectively.

We introduce two coefficients B_1 and B_2, which are

$$B_1 = \left(\beta(1-\varphi-K_b/K_s)+K_s/K_f\beta\varphi\right) + \left(-\beta+K_s/K_f\right)d\varphi, \tag{A3a}$$

$$B_2 = \left((1-\varphi_1-K_b/K_s)+K_s/K_f\beta\varphi_1\right) + \left(-1+K_s/K_f\right)d\varphi. \tag{A3b}$$

Equation (A-1a) multiplied by Equations (A-3a) and (A-3b), and neglecting the higher order terms of $d\varphi$, gives Equation (2-a). Similarly, Equation (2-b ~ d) can be derived.

Appendix B. Poroelasticity coefficients

The stiffeness and density coefficients are

$$A = (1-\varphi)K_s - \frac{2}{3}N - K_s/K_fQ_H\varphi, \tag{B1}$$

$$A_d = (1-\varphi)K_sS - \frac{2}{3}NS - Q_IR_H\left(K_s\Big/K_f^2 - 1/K_f\right) - (Q_I-R_H)K_s/K_f - K_s, \tag{B2}$$

$$N = \tilde{N} \tag{B-3}$$

$$Q_H = \frac{K_s(1-\varphi-K_b/K_s)}{1-\varphi-K_b/K_s+K_s/K_f\varphi}, \tag{B4}$$

$$Q_I = \frac{K_s(1-\varphi-K_b/K_s)}{1-\varphi-K_b/K_s+K_s/K_f\beta\varphi}, \tag{B5}$$

$$R_H = \frac{K_s\varphi}{1-\varphi-K_b/K_s+K_s/K_f\varphi}, \tag{B6}$$

$$R_I = \frac{K_s\beta\varphi}{1-\varphi-K_b/K_s+K_s/K_f\beta\varphi}, \tag{B7}$$

$$S = R_H/\varphi\left(1/\beta/K_f - 1/K_s\right) + R_I/\beta/\varphi\left(1/K_f - 1/K_s\right), \tag{B8}$$

$$\rho_{00} = (1-\varphi)\rho_s - \varphi\rho_{01}, \tag{B9}$$

$$\rho_{01} = (1-\alpha_H)\rho_f, \tag{B10}$$

$$\rho_{02} = (1-\alpha_I)\rho_f, \tag{B11}$$

$$\rho_{11} = \alpha_H\rho_f, \tag{B12}$$

$$\rho_{22} = \alpha_I\rho_f. \tag{B13}$$

Appendix C. Supplementary data

Supplementary data to this article can be found online at https://doi.org/10.1016/j.ijrmms.2020.104281.

References

1 Dvorkin J, Nur A. Dynamic poroelasticity: a unified model with the squirt and the Biot mechanisms. *Geophysics*. 1993;58(4):524–533.
2 Chapman M, Zatsepin SV, Crampin S. Derivation of a microstructural poroelastic model. *Geophys J Int*. 2002;151(2):427–451.
3 Carcione JM, Gurevich B. Differential form and numerical implementation of Biot's poroelasticity equations with squirt dissipation. *Geophysics*. 2011;76:N55–N64.
4 Tang XM, Chen XL, Xu XK. A cracked porous medium elastic wave theory and its application to interpreting acoustic data from tight formations. *Geophysics*. 2012;77(6):D245–D252.
5 Zhang L, Ba J, Carcione JM, Sun W. Modeling wave propagation in cracked porous media with penny-shaped inclusions. *Geophysics*. 2019;84(4):WA141–WA151.
6 Berryman JG, Wang HF. Elastic wave propagation and attenuation in a double-porosity dual-permeability medium. *Int J Rock Mech Min Sci*. 2000;37(1-2):63–78.
7 Pride SR, Berryman JG, Harris JM. Seismic attenuation due to wave-induced flow. *J Geophys Res: Solid Earth*. 2004;109(B1).
8 Ba J, Carcione JM, Nie JX. Biot-Rayleigh theory of wave propagation in double-porosity media. *J Geophys Res: Solid Earth*. 2011;116(B6).
9 Ba J, Zhao J, Carcione JM, Huang X. Compressional wave dispersion due to rock matrix stiffening by clay squirt flow. *Geophys Res Lett*. 2016;43(12):6186–6195.
10 Sharma MD. Wave propagation in double-porosity dual-permeability materials: velocity and attenuation. *Adv Water Resour*. 2017;106:132–143.
11 Zheng P, Ding B, Sun X. Elastic wave attenuation and dispersion induced by mesoscopic flow in double-porosity rocks. *Int J Rock Mech Min Sci*. 2017;91:104–111.

12 Müller TM, Gurevich B, Lebedev M. Seismic wave attenuation and dispersion resulting from wave-induced flow in porous rocks—a review. *Geophysics*. 2010;75(5):75A147–75A164.
13 Zhang B, Yang D, Cheng Y, Zhang Y. A unified poroviscoelastic model with mesoscopic and microscopic heterogeneities. *Chin Sci Bull*. 2019;64(17):1246–1254.
14 Jänicke R, Quintal B, Larsson F, Runesson K. Identification of viscoelastic properties from numerical model reduction of pressure diffusion in fluid-saturated porous rock with fractures. *Comput Mech*. 2019;63(1):49–67.
15 Carcione JM. *Wave Fields in Real Media. Theory and Numerical Simulation of Wave Propagation, Anisotropic, Anelastic, Porous and Electromagnetic Media*. third ed. Elsevier; 2014.
16 Durán EL, van Wijk K, Adam L, Wallis IC. Separating intrinsic and scattering attenuation in full waveform sonic logging with radiative transfer theory. *Geophys J Int*. 2018;213(2):757–769.
17 Quintal B, Caspari E, Holliger K, Steeb H. Numerically quantifying energy loss caused by squirt flow. *Geophys Prospect*. 2019;67(8):2196–2212.
18 Sun W, Ba J, Carcione JM. Theory of wave propagation in partially saturated double-porosity rocks: a triple-layer patchy model. *Geophys J Int*. 2016;205(1):22–37.
19 Zhang L, Ba J, Yin W, et al. Seismic wave propagation equations of conglomerate reservoirs: a triple-porosity structure model. *Chin J Geophys*. 2017;60(3):1073–1087.
20 Ba J, Xu W, Fu LY, Carcione JM, Zhang L. Rock anelasticity due to patchy saturation and fabric heterogeneity: a double double-porosity model of wave propagation. *J Geophys Res: Solid Earth*. 2017;122(3):1949–1976.
21 Biot MA. Theory of propagation of elastic waves in a fluid-saturated porous solid. I. Low-frequency range. *J Acoust Soc Am*. 1956;28:168–178.
22 Katz A, Thompson AH. Fractal sandstone pores: implications for conductivity and pore formation. *Phys Rev Lett*. 1985;54(12):1325.
23 Krohn CE. Sandstone fractal and Euclidean pore volume distributions. *J Geophys Res: Solid Earth*. 1988;93(B4):3286–3296.
24 Krohn CE. Fractal measurements of sandstones, shales, and carbonates. *J Geophys Res: Solid Earth*. 1988;93(B4):3297–3305.
25 Qin X, Cai J, Xu P, Dai S, Gan Q. A fractal model of effective thermal conductivity for porous media with various liquid saturation. *Int J Heat Mass Tran*. 2019;128:1149–1156.
26 Wu M, Liu J, Lv X, Shi D, Zhu Z. A study on homogenization equations of fractal porous media. *J Geophys Eng*. 2018;15(6):2388–2398.
27 Wang G, Shen J, Liu S, Jiang C, Qin X. Three-dimensional modeling and analysis of macro-pore structure of coal using combined X-ray CT imaging and fractal theory. *Int J Rock Mech Min Sci*. 2019;123:104082.
28 Wei W, Cai J, Hu X, Han Q. An electrical conductivity model for fractal porous media. *Geophys Res Lett*. 2015;42(12):4833–4840.
29 Pride SR, Masson YJ. Acoustic attenuation in self-affine porous structures. *Phys Rev Lett*. 2006;97(18):184301.
30 Norris AN. A differential scheme for the effective moduli of composites. *Mech Mater*. 1985;4(1):1–16.
31 Zimmerman RW. Elastic moduli of a solid containing spherical inclusions. *Mech Mater*. 1991;12(1):17–24.
32 Zaitsev VY, Radostin AV, Pasternak E, Dyskin A. Extracting shear and normal compliances of crack-like defects from pressure dependences of elastic-wave velocities. *Int J Rock Mech Min Sci*. 2017;97:122–133.
33 Karimpouli S, Tahmasebi P, Saenger EH. Estimating 3D elastic moduli of rock from 2D thin-section images using differential effective medium theory. *Geophysics*. 2018;83(4):MR211–MR219.
34 Han T. A simple way to model the pressure dependency of rock velocity. *Tectonophysics*. 2016;675:1–6.
35 Berryman JG. Rocks as poroelastic composites. In: *Poromechanics: A Tribute to Maurice A. Biot, Proceedings of the Biot Conference on Poromechanics, Université Catholique de Louvain, Louvain-la-Neuve, Belgium*. 1998:11–16.
36 Berryman JG. Single-scattering approximations for coefficients in Biot's equations of poroelasticity. *J Acoust Soc Am*. 1992;91(2):551–571.
37 Berryman JG, Pride SR, Wang HF. A differential scheme for elastic properties of rocks with dry or saturated cracks. *Geophys J Int*. 2002;151(2):597–611.
38 Gassmann F. *Über die Elastizität poröser Medien: Vierteljahrsschriftder Naturforschenden Gesellschaft in Zürich*. vol. 96. 1951:1–23.
39 Sakhaee-Pour A, Li W. Fractal dimensions of shale. *J Nat Gas Sci Eng*. 2016;30:578–582.
40 Rieu M, Perrier E. Fractal models of fragmented and aggregated soils. In: *Revival: Fractals in Soil Science*. CRC Press; 1998:169–202, 2017.
41 Zhou JX, Zhang XZ, Knobles DP. Low-frequency geoacoustic model for the effective properties of sandy seabottoms. *J Acoust Soc Am*. 2009;125(5):2847–2866.
42 Li ZL, Zhang RH. A broadband geoacoustic inversion scheme. *Chin Phys Lett*. 2004;21(6):1100.
43 Knobles DP, Yudichak TW, Koch RA, Cable PG, Miller JH, Potty GR. Inferences on seabed acoustics in the East China Sea from distributed acoustic measurements. *Ieee J Oceanic Eng*. 2006;31(1):129–144.
44 Richardson MD, Briggs KB, Bibee LD, et al. Overview of SAX99: environmental considerations. *Ieee J Oceanic Eng*. 2001;26(1):26–53.
45 Hines PC, Osler JC, Scrutton JG, Halloran LJ. Time-of-flight measurements of acoustic wave speed in a sandy sediment at 0.6–20 kHz. *Ieee J Oceanic Eng*. 2010;35(3):502–515.
46 Buckingham MJ. Compressional and shear wave properties of marine sediments: comparisons between theory and data. *J Acoust Soc Am*. 2005;117(1):137–152.
47 Isakson MJ, Neilsen TB. The viability of reflection loss measurement inversion to predict broadband acoustic behavior. *J Acoust Soc Am*. 2006;120(1):135–144.
48 Chotiros NP, Isakson MJ. A broadband model of sandy ocean sediments: Biot–Stoll with contact squirt flow and shear drag. *J Acoust Soc Am*. 2004;116(4):2011–2022.